neurogenetics (2019) 20:117–127
https://doi.org/10.1007/s10048-019-00576-3

ORIGINAL ARTICLE

Linkage analysis and whole exome sequencing reveals *AHNAK2* as a novel genetic cause for autosomal recessive CMT in a Malaysian family

Shelisa Tey[1] · Nortina Shahrizaila[2] · Alexander P. Drew[3,4] · Sarimah Samulong[1] · Khean-Jin Goh[2] · Esra Battaloglu[5] · Derek Atkinson[6] · Yesim Parman[7] · Albena Jordanova[6] · Ki Wha Chung[8] · Byung-Ok Choi[9] · Yi-Chung Li[10] · Michaela Auer-Grumbach[11] · Garth A. Nicholson[3,4,12] · Marina L. Kennerson[3,4,12] · Azlina Ahmad-Annuar[1]

Received: 27 November 2018 / Accepted: 3 April 2019 / Published online: 22 April 2019

Abstract

Charcot-Marie-Tooth (CMT) disease is a form of inherited peripheral neuropathy that affects motor and sensory neurons. To identify the causative gene in a consanguineous family with autosomal recessive CMT (AR-CMT), we employed a combination of linkage analysis and whole exome sequencing. After excluding known AR-CMT genes, genome-wide linkage analysis mapped the disease locus to a 7.48-Mb interval on chromosome 14q32.11–q32.33, flanked by the markers rs2124843 and rs4983409. Whole exome sequencing identified two non-synonymous variants (p.T40P and p.H915Y) in the *AHNAK2* gene that segregated with the disease in the family. Pathogenic predictions indicated that p.T40P is the likely causative allele. Analysis of AHNAK2 expression in the AR-CMT patient fibroblasts showed significantly reduced mRNA and protein levels. AHNAK2 binds directly to periaxin which is encoded by the *PRX* gene, and *PRX* mutations are associated with another form of AR-CMT (CMT4F). The altered expression of mutant AHNAK2 may disrupt the AHNAK2-PRX interaction in which one of its known functions is to regulate myelination.

Keywords Inherited neuropathy · AHNAK2 · Autosomal recessive CMT

Introduction

Inherited peripheral neuropathies are a group of disorders of the peripheral nervous system with heterogenous clinical phenotypes involving a wide range of genes. Charcot-Marie-Tooth disease (CMT) is the most common inherited peripheral neuropathy with a prevalence of 1 in 2500 [1]. CMT patients typically present with progressive distal muscle weakness and atrophy, foot deformities, sensory loss and reduced reflexes. The classification of CMT has traditionally been based on neurophysiological recordings and the mode of inheritance [2]. However, the plethora of known CMT genes and subsequent genetic testing has further defined the disease classifications.

Almost 90 genes have been identified for CMT and associated neuropathies [3]. Genes for autosomal recessive CMT (AR-CMT) were mainly identified through studies with large pedigrees and specific populations, whilst next-generation sequencing in small nuclear families has accelerated gene discoveries including mutations in *HINT1*, *IGHMBP2* and *MCM3AP* [4–6, respectively].

In this study, we used a combination of linkage analysis and whole exome sequencing to identify the causal gene in a Malaysian family with demyelinating AR-CMT.

Marina L. Kennerson and Azlina Ahmad-Annuar contributed equally to this work.

Electronic supplementary material The online version of this article (https://doi.org/10.1007/s10048-019-00576-3) contains supplementary material, which is available to authorized users.

✉ Marina L. Kennerson
marina.kennerson@sydney.edu.au

✉ Azlina Ahmad-Annuar
azlina_aa@um.edu.my

Extended author information available on the last page of the article

Materials and methods

Subjects

CMT861 family

Eighteen family members of Indian ethnicity were recruited which included two brothers with CMT. Genomic DNA was extracted from peripheral blood using the QIAamp DNA Blood Maxi Kit (Qiagen, Hilden, Germany) at the University of Malaya for the family members and Indian controls, whilst the PureGene Kit was used in the ANZAC laboratory for the normal controls. Controls comprised of healthy individuals free of any neurological disorder. Ethics approval from the University of Malaya Medical Centre and the Sydney Local Health District Human Ethics Research Committee (Concord Hospital, Sydney) was obtained and all participants provided written consent.

Linkage and haplotype mapping

Using the EasyLinkage package, simulation studies were performed using FastLINK to determine the maximum theoretical LOD score and linkage power of the family [7]. The Golden Gate Linkage V Panel was initially used to genotype six family members (III:9, III:10, IV:6, IV:7, IV:8, IV:9) for genome-wide linkage analysis. Multipoint linkage was performed using the MERLIN program [8]. For the parametric linkage analysis, fully penetrant autosomal recessive inheritance was assumed with a disease allele frequency of 0.001.

Suggestive linkage peaks with LOD scores > 2 were further analysed with microsatellite markers, and two-point and multipoint linkage analyses were performed on 18 members of the family using the MLINK and LINKMAP program of the Linkage Package [9]. Microsatellite marker information was retrieved from the Rutgers Map Browser (build 37) [10], and additional SNP markers were selected from the whole exome sequencing variant dataset of the proband.

Whole exome sequencing

Whole exome sequencing (WES) was performed on genomic DNA (2.5 μg) in five family members of CMT861 (III:9, III:10, IV:7, IV:8, IV:9) at Axeq Technologies (Seoul, South Korea) as previously described [11].

Detecting runs of homozygosity

Runs of homozygosity (ROH) were determined using SNP genotypes from the WES dataset. The Linkdatagen Perl script (release 20130704) was used to generate input files using PLINK [12, 13]. Annotation files were prepared with HapMap II CEU genotypes, and a bin size of zero was chosen to maximise the number of SNPs included in the analysis. SNPs that were missing, not annotated, or had a read depth of less than 10 were excluded. Using the default parameters, PLINK scanned the genome with a window of 50 consecutive SNPs to determine ROH. One heterozygous SNP was allowed in each window and the overlap between the sliding windows was set at 5%. The maximum gap allowed in between SNPs was 1000 kb and only regions with a minimum of a hundred consecutive homozygous SNPs were selected. Overlapping homozygous segments were compared pairwise within the family members and were considered to be shared between individuals if 95% of the variants within the homozygous segments matched. The ROH shared by the affected brothers and absent in the unaffected family members were prioritised for further analysis.

Candidate variants from WES

The web-based Galaxy platform (http://galaxyproject.org/) was used to perform a series of filtering steps with the WES data [14, 15]. Shared variants between the two affected brothers (IV:7 and IV:9) were selected, and common variants were excluded by comparing the shared patient data with exome datasets of unrelated neurologically normal males of Caucasian (20) and Indian (one) ethnicities.

Candidate variants were further prioritised based on the following criteria: (1) localization within regions defined by linkage and runs of homozygosity; (2) variants having a minor allele frequency less than 1%, in the homozygous state; and (3) non-synonymous variants. The candidate variants fulfilling these criteria were validated using Sanger sequencing and then screened using in-house controls (754 normal controls, including 132 of Indian ethnicity), with established high-resolution melting (HRM) protocols [16]. In addition, exome datasets from families of European, Korean and Taiwanese ethnicities were queried for variants in candidate genes. The variants identified were tested for segregation with the disease phenotype in these families. The variants reported in *AHNAK2* are annotated using the accession numbers NM_138420 and NP_612429.

Gene expression studies

Skin biopsies from patients (IV:7, IV:9) and five male controls were cultured in FDMEM containing 10% (*v*/*v*) inactivated foetal bovine serum, 200 mM L-glutamine and 5000 U/mL Penicillin/Streptomycin. RNA extractions from fibroblasts were performed using the NuclearSpin RNA Kit (Macherey-Nagel). Total RNA (500 ng to 1 μg) was reverse transcribed using the iScript cDNA Synthesis Kit (Bio-Rad). A Taqman gene expression assay (Fisher Biotech) using the comparative $2^{-\Delta\Delta Ct}$ method was used to quantitate the relative expression of *AHNAK2* (Hs00292832_M1) between patients and

controls [17]. The *HPRT1* (Hs02800695_m1) gene was used as the endogenous control for normalising the target gene expression.

Immunocytochemistry, confocal imaging and image analysis

Fibroblast cells were fixed with 4% (*w*/*v*) paraformaldehyde (PFA) for 15 min at room temperature, then washed with 1× PBS. Blocking was performed with 0.1% (*v*/*v*) Triton X-100 for 5 min, followed by 5% (*w*/*v*) bovine serum albumin (BSA) for 30 min at room temperature. The cells were incubated with the rabbit anti-human carboxyl terminal AHNAK2 primary antibody (HPA004145, Atlas Antibodies) at a dilution of 1:100 (in 1% (*w*/*v*) BSA) at room temperature for 3 h, and washed twice with 1× PBS. The secondary antibody, Alexa 488-labelled anti-rabbit IgG antibody (A-11070, Molecular Probes), was used at a dilution of 1:200 (in 1× PBS) and incubated at room temperature for 1 h, and washed in 1× PBS. The cells were stained with Hoechst (H3570, Molecular Probes) for nuclear staining. Cells were viewed under a Leica TCS SP5 II confocal microscope, and images were captured with LAS X software. Images (10 or more) were taken for both controls and patients, from three independent experiments. Image analysis was performed using the Image Pro Plus software (Media Cybernetics). The average AHNAK2 intensity per image was measured by quantifying the intensity of the AHNAK2 signal and dividing the value over the number of cells (counted by DAPI staining). The average AHNAK2 intensity per number of cells across all images was then compared between the control and patient groups. The same procedure was followed to stain for actin using the Phalloidin antibody conjugated with an Alexa Fluor 546 dye (Molecular Probes) and Hoechst as above. The Student's *t* test was used to compare the two groups, where a *p* value of less than 0.05 was considered significant.

Results

Our previous study on a Malaysian CMT cohort showed that in 40% of cases, no mutations were detected in the common CMT genes (*PMP22*, *GJB1*, *MPZ*, *MFN2*) [18]. This study investigated one unsolved family (CMT861) with two affected brothers (IV:7 and IV:9) from a consanguineous marriage (Fig. 1).

Clinical features (CMT861)

The proband (IV:7) first presented to the orthopaedic surgeons at the age of 16 with a 4-year history of gait difficulties. He was subsequently referred to the neurology clinic. Neurological examination of the upper limbs revealed atrophy of the small muscles of his hands and weakness (MRC grade 3/5) of his abductor pollicis brevis and first dorsal interossei muscles. Upper limb reflexes were absent and sensation was intact. Examination of the lower limbs revealed increased tone but no sustained ankle clonus. There was wasting of the small muscles of the feet and tibialis anterior bilaterally. Ankle dorsiflexion was reduced in strength (MRC grade 2/5). Ankle reflexes were absent but knee reflexes were brisk. Vibration sense was absent in the toes, reduced at the ankles and present at the knees. Pinprick sensation and proprioception was intact. Nerve conduction studies (NCS) revealed either absent or markedly reduced amplitude of the sensory nerve action potentials (Table 1). Compound muscle action potentials (CMAPs) were un-recordable in the distal lower limb muscles and reduced in amplitude in the upper limbs. Motor conduction velocities were reduced and were within the demyelinating ranges (median 34 m/s, ulnar 36 m/s). Distal motor latencies were prolonged and *F* wave latencies were delayed. Needle electromyography showed evidence of chronic denervation changes in the distal limb muscles. In view of the increased lower limb tone and brisk knee reflexes, MRI of the whole spine was performed and found to be normal.

His younger brother (IV:9) was noted to have similar symptoms and was examined at the age of 15. He described gait difficulties since 13 years of age with frequent falls as a result of tripping over his foot. He had a high steppage gait, and unlike his brother, his muscle tone was normal. There was reduced muscle strength in the distal muscles of his upper (finger abduction MRC grade 4/5) and lower limbs (dorsiflexion MRC grade 3/5). Reflexes were absent at the ankles, brisk at the knees and depressed in the upper limbs. Vibratory sense was absent at the toes but pain and proprioception was intact. NCS findings were similar to his older brother's scores, with features of demyelinating sensorimotor neuropathy with secondary axonal changes (Table 1). Both parents and two unaffected siblings were also examined and their nerve conduction studies were normal.

Mapping a new locus for demyelinating AR-CMT to chromosome 14q32.11–q32.3

The pedigree for CMT861 is shown in Fig. 1. Simulation studies modelling a linked microsatellite marker (four-allele) and a SNP marker (two-allele) in the pedigree gave maximum theoretical two-point LOD scores of 1.75 and 1.45 at $\theta = 0$, respectively (Supp. Table 1). Analysis of a genome-wide linkage scan in six of the family members achieved a maximum multipoint LOD score of 2.05 for chromosomes 3, 11, 12, 14, 19 and 20, with two peaks identified on chromosome 11 (Supp. Table 2 and Suppl. Fig. 1). An additional suggestive linkage peak was found on chromosome 7 with a multipoint LOD score approaching 2 (LOD = 1.94). Fine-mapping using

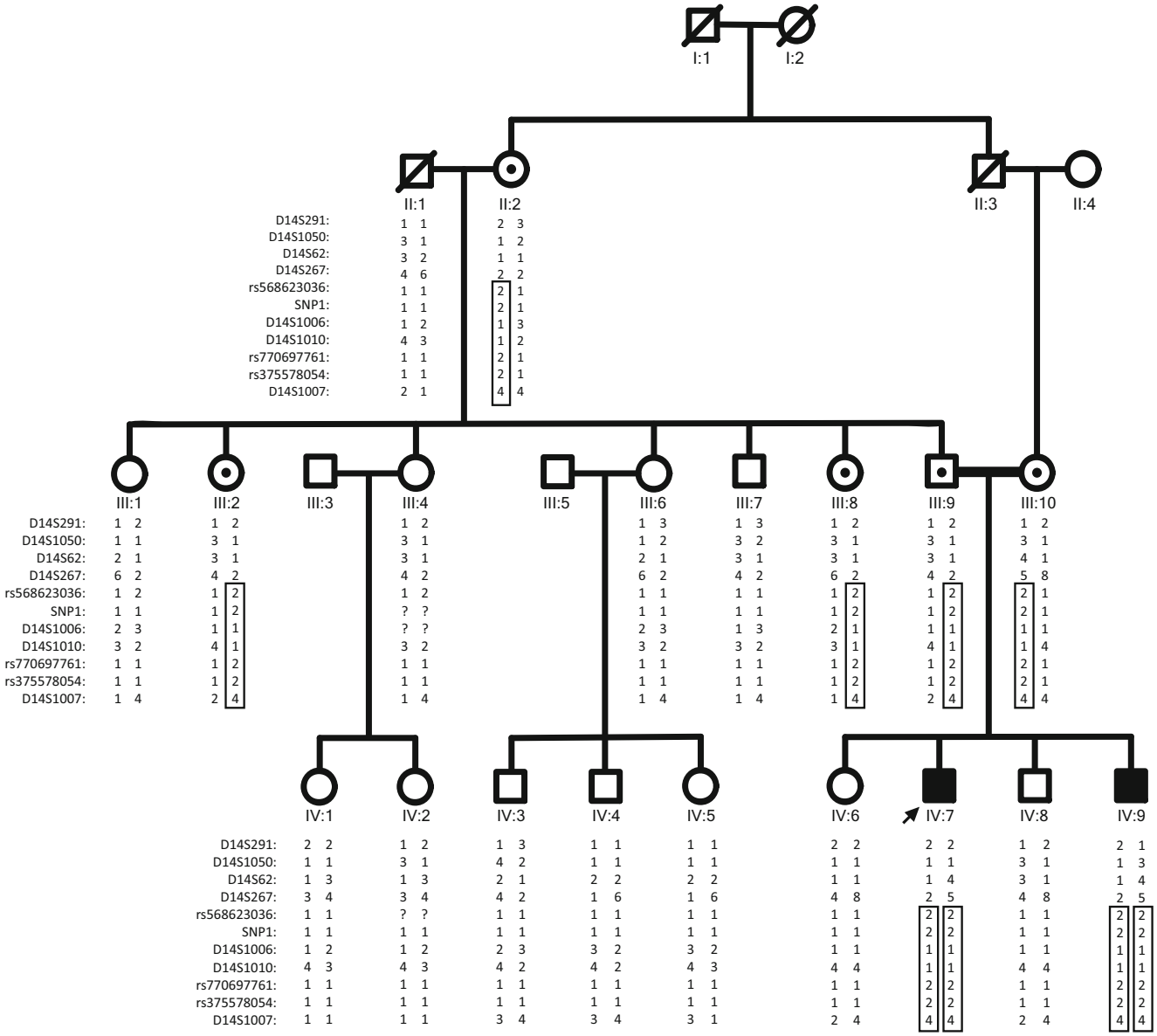

Fig. 1 Extended haplotype analysis of markers on chromosome 14q32.11–q32.33. Females and males are represented by circles and squares, respectively. Solid symbols indicate affected individuals. Symbols with a black dot indicate a carrier. Marker alleles are listed below the individuals and ordered from centromere to telomere. The haplotype outlined by the box defines the haplotype segregating with the disease. Haplotype analysis shows that the affected males are homozygous for the disease haplotype (2-2-1-1-2-2-4). A recombination event identified in the affected brothers between marker D14S267 and rs568623036 defined D14S267 as the proximal flanking marker. The suggestive linkage region is refined to the interval between marker D14S267 and the distal end of chromosome 14q. This corresponds to an 8.12-Mb candidate interval

informative microsatellite markers excluded chromosomes 3, 7, 11, 19 and 20 when tested in all the family members (Suppl. Fig. 2). Chromosome 12 was not excluded; however subsequent analysis showed that there was no shared ROH or candidate gene variants (missense or truncation) in that region. This suggested that the locus was less likely to be disease-causing and was therefore not prioritised for further analysis in this study.

No ROH were detected which overlapped with the linkage peaks on chromosomes 3, 7, 19 and 20. An ROH was detected on chromosome 11, spanning approximately 2.63 Mb (chr11 65,294,223–67,924,904), (Suppl. Fig. 3). However, within this region, a large internal portion was shared with the parents and the affected brothers between markers rs7107453 and rs2286163. Flanking the internal region were two shorter ROHs exclusive to the affected brothers corresponding to a 0.25-Mb interval between markers rs1622368 and rs7107453 (0.25 Mb) and the second 0.13-Mb interval between the markers rs2286163 and rs7121441. The internal ROH was excluded for pathogenicity based on both parents possessing the ROH and

Table 1 Nerve conduction study of affected individuals

	Proband IV:7 (CMT861)			IV:9 (CMT861)		
Sensory studies	Amplitude (μV)	Velocity (m/s)		Amplitude (μV)	Velocity (m/s)	
Median	3.2	32		NR	NR	
Ulnar	NR	NR		NR	NR	
Radial	5.4	33		NR	NR	
Sural	NR	NR		NR	NR	
Motor studies	Distal latency (ms)	Amplitude (mV)	Velocity (m/s)	Distal latency (ms)	Amplitude (mV)	Velocity (m/s)
Median	5.6	4.2	34	7.2	1.9	28
Ulnar	4.2	1.8	36	5.1	4.3	32
Peroneal	NR	NR	NR	NR	NR	NR
Tibial	NR	NR	NR	NR	NR	NR

NR no response

being unaffected. The shorter ROH shared by the brothers were excluded with statistical significance after performing multipoint linkage analysis with microsatellite markers across the suggestive linkage peak (Suppl Fig. 2c).

The linkage peak on chromosome 14q32.11–q32.33 mapped to a 15.79-Mb interval flanked by the markers rs4904745 and rs1989750 (Fig. 2a, b). Fine mapping using two-point analysis of genotyped microsatellite markers showed the disease locus recombined with D14S291, D14S1050, D14S62 and D14S267 at zero recombination (Suppl. Table 3). Multipoint linkage analysis confirmed exclusion of the interval between the markers D14S291 and D14S267 and maintained a LOD score > 2.0 between the markers D14S267 and D14S1007 (Fig. 2c). Haplotype analysis showed that the two affected sons were homozygous for an 8.12-Mb haplotype block spanning rs568623036 to D14S1007 (2-2-1-1-2-2-4) which was inherited from each carrier parent (III:9 and III:10) (Fig. 1). Using WES data of the proband (IV:7), an affected brother (IV:9), an unaffected brother (IV:8) and the parents (III:9 and III:10), a ROH shared between the affected brothers further defined a 7.48-Mb interval flanked by the markers rs2124843 and rs4983409 (Fig. 2c). The ROH was present only in the affected brothers and overlapped with the linkage interval (Fig. 2c). Based on excluding other chromosomal linkage peaks, haplotype and ROH segregation and multipoint LOD scores exceeding the simulated maximum LOD score for the family, this evidence supported the region on chromosome 14q32.11–32.33 as a novel and likely disease locus in CMT861.

WES identifies a mutation in *AHNAK2*

WES of the proband (IV:7) excluded mutations in the known peripheral neuropathy genes. Filtering for shared variants between the affected brothers identified 51,653 candidate variants. Further filtering against exome data from unaffected family members reduced the number of candidate variants in the brothers to 3278. These variants were further reduced to 2757 by filtering against WES data from 20 Caucasian controls and an ethnically matched Indian control. The subsequent selection criteria to prioritise candidate variants (homozygous, non-synonymous variants with a MAF < 1%) identified eight candidates (Supp. Table 4).

Two of the eight candidate variants were exonic (c.A118C and c.C2743T) and localised within the *AHNAK2* gene (Fig. 3a). Both of the variants were validated by Sanger sequencing and fully segregated with the disease phenotype in family CMT861 (Fig. 3b and Suppl. Fig. 4). The novel missense variant (c.A118C) corresponds to a p.T40P substitution in exon 3, and is absent in 1508 control chromosomes screened by HRM analysis. This variant is also unreported in the dbSNP150 EVS, ExAC, NHLBI and 1000 Genomes databases. The second variant located in exon 7 (c.C2743T, p.H915Y) is a reported SNP (rs375578054) with a MAF of 0.1%. It is absent in 400 control chromosomes screened by HRM. The variant rs375578054 has been reported in the heterozygous state in 5 out of 5008 chromosomes (0.1%) and in 19 out of 120,144 chromosomes (0.02%) in the 1000 Genomes and ExAC databases, respectively.

The *AHNAK2* gene encodes a protein with a PDZ domain at the N-terminal (amino acids 112–191) and a large central region of long repetitive motifs located outside the PDZ domain (amino acids 674–4742). The wild-type nucleotide at c.A118 is highly constrained with a GERP score of 3.21, Phastcon score of 0.99 and PhyloP score of 2.63. The CADD score [19] of 23.3 indicates a nucleotide substitution at this position is in the top 1% of most deleterious changes in the genome. The p.T40P substitution is predicted to be damaging by in silico protein prediction programs (SIFT score = 0,

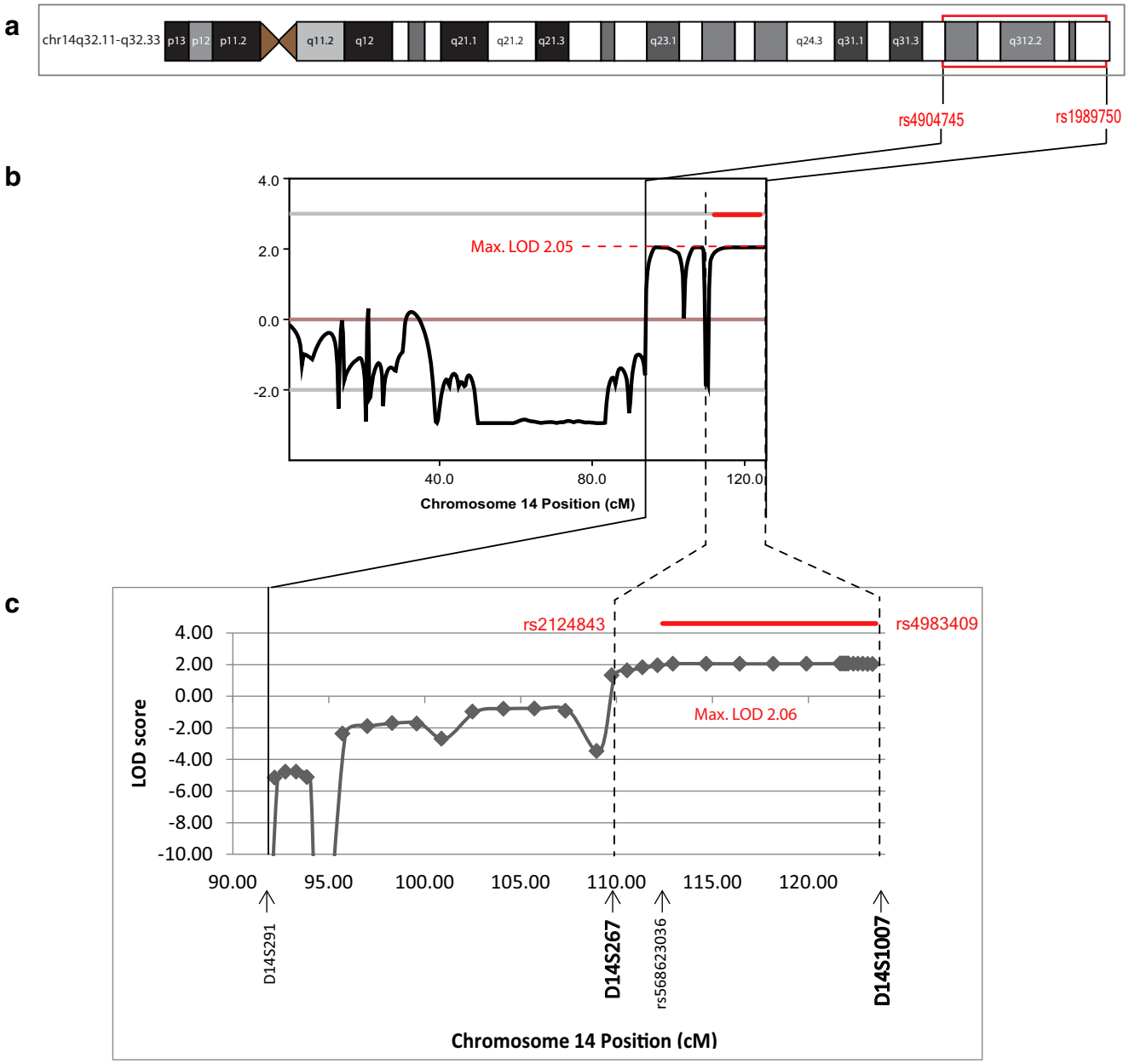

Fig. 2 Combined LOD score and ROH data support an overlapping region on chromosome 14q32.11–q32.33. **a** Ideogram showing the location of the candidate region on chromosome 14. **b** Multipoint LOD score likelihood curves from the genome wide scan defined a suggestive 15.79-Mb linkage region flanked by the markers markers rs4904745 and rs1989750. **c** Multipoint likelihood curves generated from microsatellite and SNP markers further refined the suggestive linkage peak to an 8.12-Mb region between D14S267 and D14S1007 (bold). The shared haplotype block spanned rs568623036 to D14S1007. The red bar represents the ROH between markers rs2124843 and rs4983409 which reduced the candidate interval from 8.12 to 7.48 Mb

PolyPhen2 score = 0.998). The wild-type nucleotide for the c.C2473T variant (p.H915Y) has a GERP score of 0.69, PhastCons score of 0, PhyloP score of 0.39 and CADD score of 13.98 indicating a low level of constraint. The p.H915Y substitution is predicted to have a milder effect (SIFT score = 0.065, PolyPhen2 score = 0.995). The pathogenic predictions therefore support the p.T40P substitution is more likely to be damaging when compared to the p.H915Y substitution.

Unsolved neuropathy families queried for *AHNAK2* mutations

To identify other possible families with *AHNAK2* mutations, in-house WES datasets of unsolved IPN families ($N = 115$), the Genesis database, as well as 54 European, 425 Korean and 135 Taiwanese unsolved IPN patients were queried (Supp. Table 5). A heterozygous variant in exon 3 (c.C151T, p.R51W) was excluded by segregation analysis. A

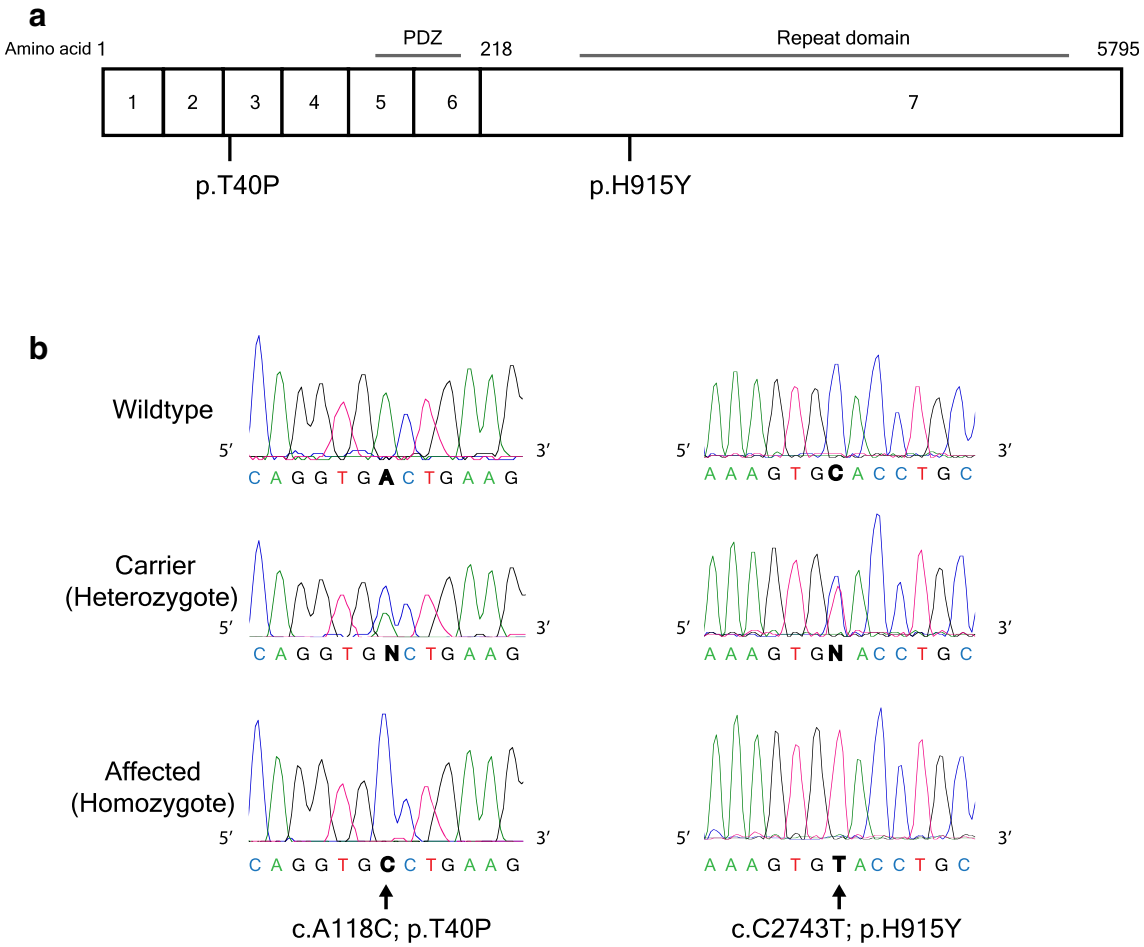

Fig. 3 Schematic figure of the *AHNAK2* gene and sequence electropherograms of the mutations. **a** Structure of *AHNAK2*. The boxes represent the coding exons. Amino acid residues 1 to 217 cover exons 1 to 6 and residues 218 to 5795 span exon 7. The p.T40P localises within exon 3 and p.H915Y is in exon 7. AHNAK2 has a PDZ domain from amino acids 112–191 and a repeat domain from amino acids 674–4742. **b** Sequence traces for wild-type control, heterozygous carrier and homozygous patient for c.A118C (p.T40P) and c.C2743T (p.H915Y) are shown

heterozygous variant in exon 5 (c.G412A, p.V138I) in a Taiwanese patient was excluded as it was also present in 4 out of 997 normal individuals, as reported in a national control exome database (https://taiwanview.twbiobank.org.tw/index). Segregation analysis of two heterozygous exon 7 variants (c.A14187G, p.I4729M and c.C1342T, p.R448W) in a single European HMSN II family also excluded these variants. Segregation analysis was not possible to evaluate a variant in exon 5 (c.C386G, p.T129R) found in a late onset motor-predominant CMT2 patient.

In a Korean cohort, a heterozygous variant (c.C16925G, p.S5642C in a CMT2 family) and a homozygous variant (c.A5023G, p.K1675E in a dHMN family, FC159) both localising to exon 7 in unrelated families were shown to segregate with the phenotype in the respective families. Fibroblasts were not available for the p.S5642C family for further analysis, and the p.K1675E variant was excluded as it is reported as a rare homozygous polymorphism in various ethnicities in the ExAC database. Segregation analysis was not possible for two other families, one with compound heterozygous variants p.A203P and p.G450S and the second with two heterozygous variants (p.R1144W, p.K1492R) and one homozygote (p.L3217P) variant.

Altered *AHNAK2* gene expression is observed in AR-CMT patient fibroblasts

To assess the functional impact of the *AHNAK2* mutations, gene expression studies were performed to investigate mRNA and protein levels in fibroblasts from both affected brothers. Fibroblasts from both brothers showed a highly significant reduction in *AHNAK2* expression when compared to control fibroblasts ($p < 0.001$) (Fig. 4a). Immunostaining of fibroblasts with the p.T40P mutation showed a highly significant reduction in AHNAK2 protein expression ($p < 0.001$) when compared to controls (Fig. 4b, c). In comparison, actin expression levels were not significantly different in patient fibroblasts compared to controls (Fig. 4d, e), indicating that

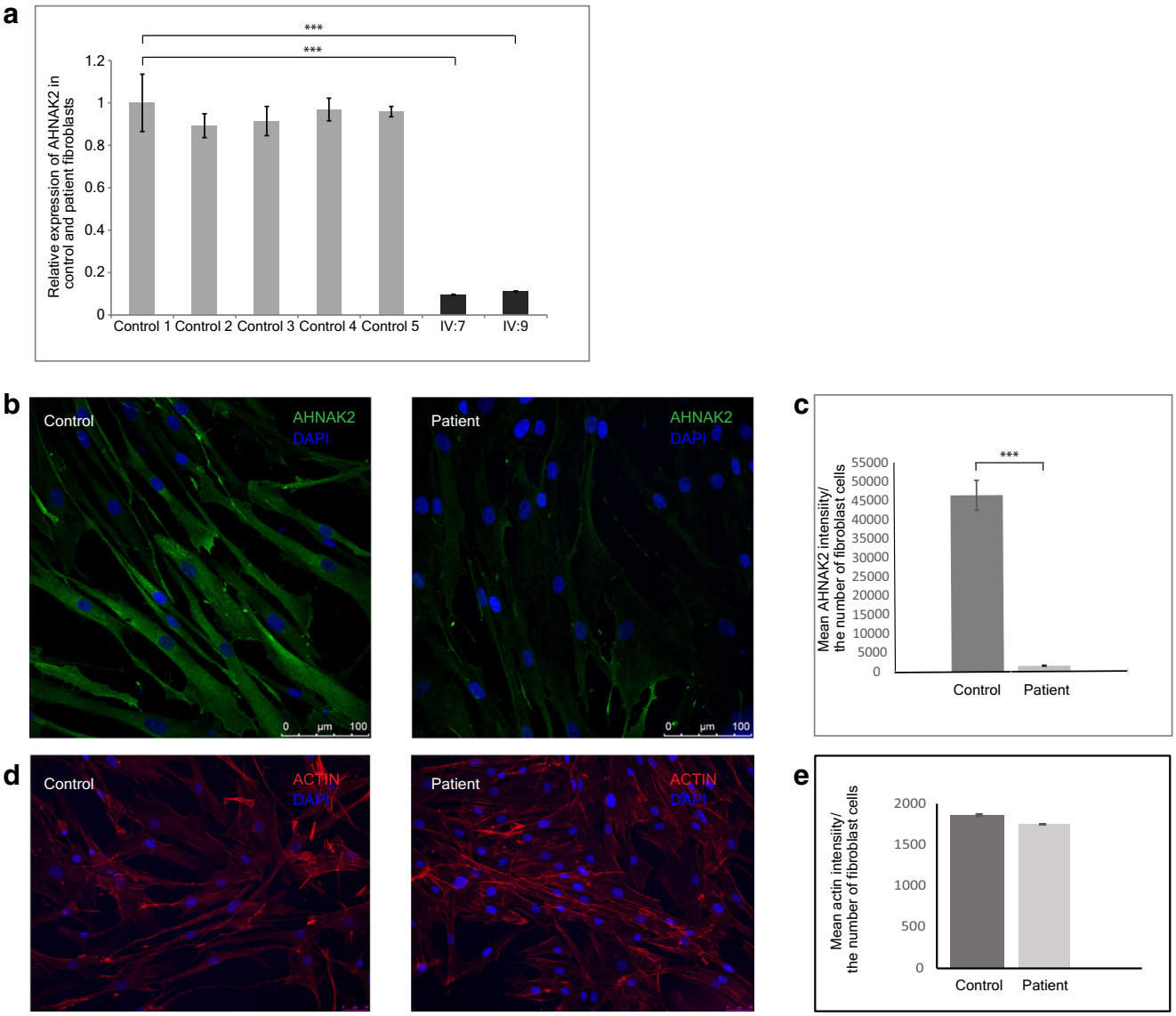

Fig. 4 Reduced AHNAK2 expression in patient fibroblasts at the mRNA and protein level. **a** Relative expression of *AHNAK2* mRNA in patient fibroblasts with the p.T40P, p.H915Y mutations compared to controls. Bars show the mean mRNA levels of *AHNAK2* normalised to HPRT (± SEM; error bars) relative to control 1. A significant 8.9–10.5-fold decrease in *AHNAK2* expression in both patients was observed, for IV9 and IV:7, respectively ($p < 0.001$). **b** Wild type and patient p.T40P, p.H915Y fibroblasts were immunostained with anti-AHNAK2 antibodies (green) and DAPI (blue). AHNAK2 has a clear perinuclear and cytoplasmic expression in the control fibroblasts which is not apparent in the patient fibroblasts. **c** Quantitation of AHNAK2 expression (fluorescence intensity ± SEM; error bars) between the control and patient fibroblasts. ***$p < 0.001$. **d** Wild type and patient p.T40P, p.H915Y fibroblasts were immunostained with anti-actin antibodies (red) and DAPI (blue). **e** Quantification of actin expression (fluorescence intensity ± SEM; error bars) between the control and patient fibroblasts

the reduction of protein levels in the patient fibroblasts was specific to *AHNAK2*.

Discussion

We have mapped a new locus for AR-CMT with neurophysiological features supportive of demyelinating neuropathy in a Malaysian Indian family and identified variants in the *AHNAK2* gene in which one (p.T40P) is likely to be causative. There are several lines of evidence supporting *AHNAK2* as the likely causative gene in this family: (1) two complementary mapping approaches supported mapping the disease locus for CMT861 to a region on chromosome 14q32.22–q32.33; (2) whole exome sequencing excluded known CMT genes; (3) the homozygous mutation p.T40P is absent in published databases, ethnically matched controls and in-house control exomes; and (4) expression studies in patient fibroblasts showed significantly reduced levels of AHNAK2.

AHNAK2 is a large gene with over 200 non-synonymous heterozygous variants in exons 1–6 and over 3000 non-synonymous heterozygous and homozygous variants in exon 7 as reported in 1000 Genomes, ExAC and NHLBI EVS databases. Due to the large number of variants in exon 7, careful interpretation of candidate variants within this variable region should be assessed by segregation studies, control screening and functional analysis. Interestingly, there is a rare heterozygous variant (p.T40I, MAF 0.001) reported in a single individual, at the same amino acid residue as the affected brothers in family CMT861 (p.T40P). Based on the frequency of this variant, it is possible that this individual is a carrier for an *AHNAK2* mutated allele which is non-pathogenic in the heterozygous state; however due to de-identified information for this sample in the ExAC database, further evaluation is not possible.

Recently, a comprehensive study in a large Pakistani cohort of healthy consanguineous families indicated that rare homozygous variants representing loss-of-function (LOF) genotypes that may have been presumed to be pathogenic, can be found in normal healthy individuals [20]. Such findings can confound the interpretation of homozygous variants for autosomal recessive diseases. In particular for CMT861, we reviewed the datasets reported in this study as this family is of Indian ethnicity and may share genetic lineage with the Pakistani cohort studied. No *AHNAK2* mutations were reported, which further support the argument that the p.T40P and p.H915Y homozygous mutations have only been observed in affected individuals.

Functional data on *AHNAK2* expression provides evidence suggesting how the mutations may be causing the phenotypes in CMT861. We postulate that the p.T40P and p.H915Y are in linkage disequilibrium, and may play a synergistic role in disease pathogenesis or alternatively, p.H915Y is a benign polymorphism in LD with the p.T40P causative allele. Presently, it is not clear how the point mutation leads to reduced mRNA and protein expression; however, other studies have reported similar effects [21, 22]. One possibility may be the introduction of a microRNA binding site or changes to the chromatin structure which hinders access of transcriptional machinery to the regulatory domains controlling *AHNAK2* gene expression.

AHNAK2 encodes a 616-kDa protein [23], in which the function is poorly understood. Mutations in *AHNAK1* have been reported in a kindred with recessive Hirshsprung disease but these patients also carried mutations in the *ENDRB* gene which is thought to modulate disease penetrance through interactions with *AHNAK2* [24]. Recently, a novel insertion in exon 7 (c.6436_6437insGG:p.L2146fs) was identified in a Saudi Arabian family with dysmorphic features and skeletal abnormalities [25]. It was assumed to be pathogenic by in silico prediction tools.

In mice, Ahnak2 co-localises with Ahnak1 in skeletal muscle [23, 26] and are thought to have similar roles in regulating calcium channels and interacting with multiple cytoskeleton proteins such as dysferlin, annesin 2, myoferlin, actin and dystrophin [23, 26–30]. Homozygous *Ahnak1* knockout mice show no obvious phenotype at birth or during development, but as the age of the mice studied was not stated, the onset of a neuropathic phenotype may not have been observed [23]. Alternatively, the lack of disease phenotype may be due to a possible compensatory role of *Ahnak2* [23, 28]. As yet, there are no reported *Ahnak2* knockout mice.

Crystallography studies on AHNAK2 and periaxin (PRX) have indicated that these proteins form heterodimers through their PDZ domains [30]. Periaxin is essential for myelin sheath maintenance, and mutations in *PRX* are known to cause demyelinating Charcot-Marie-Tooth disease type 4F and Dejerine-Sottas disease (CMT3) [31–33]. Through dimerisation with PRX, AHNAK2 may be involved in similar myelination maintenance roles. Mutations in *AHNAK2* could therefore be hypothesised to disrupt this interaction and possibly lead to a demyelinating phenotype, as observed in the AR-CMT family CMT861. Importantly, the binding to PRX is specific for AHNAK2 and not AHNAK1; therefore, the loss of AHNAK2 in our patients may not be compensated by AHNAK1. Other studies have also shown a role for AHNAK2 in stress-induced FGF1 secretion [34], where FGF1 is involved in neurite outgrowth of mouse cochlear ganglion cells [35].

In summary, this study highlights a new avenue for understanding the role of *AHNAK2* and expands the genetic aetiology of AR-CMT.

Compliance with ethical standards

Ethical approval All procedures performed in studies involving human participants were in accordance with the ethical standards of the institutional and/or national research committee and with the 1964 Helsinki declaration and its later amendments or comparable ethical standards.

Informed consent Informed consent was obtained from all individual participants included in the study.

References

1. Brennan KM, Bai Y, Shy ME (2015) Demyelinating CMT—what's known, what's new and what's in store? Neurosci Lett 596:14–26
2. Harding AE, Thomas PK (1980) The clinical features of hereditary motor and sensory neuropathy types I and II. Brain 103:259–280
3. Timmerman V, Strickland A, Züchner S (2014) Genetics of Charcot-Marie-Tooth (CMT) disease within the frame of the human genome project success. Genes 5:13–32
4. Zimon M, Baets J, Almeida-Souza L, De Vriendt E, Nikodinovic J, Parman Y, Battaloglu E, Matur Z, Guergueltcheva V, Tournev I, Auer-Grumbach M, De Rijk P, Petersen BS, Muller T, Fransen E, Van Damme P, Loscher WN, Barisic N, Mitrovic Z, Previtali SC,

Topaloglu H, Bernert G, Beleza-Meireles A, Todorovic S, Savic-Pavicevic D, Ishpekova B, Lechner S, Peeters K, Ooms T, Hahn AF, Zuchner S, Timmerman V, Van Dijck P, Rasic VM, Janecke AR, De Jonghe P, Jordanova A (2012) Loss-of-function mutations in HINT1 cause axonal neuropathy with neuromyotonia. Nat Genet 44:1080–1083

5. Cottenie E, Kochanski A, Jordanova A, Bansagi B, Zimon M, Horga A, Jaunmuktane Z, Saveri P, Rasic Vedrana M, Baets J, Bartsakoulia M, Ploski R, Teterycz P, Nikolic M, Quinlivan R, Laura M, Sweeney Mary G, Taroni F, Lunn Michael P, Moroni I, Gonzalez M, Hanna Michael G, Bettencourt C, Chabrol E, Franke A, von Au K, Schilhabel M, Kabzińska D, Hausmanowa-Petrusewicz I, Brandner S, Lim Siew C, Song H, Choi B-O, Horvath R, Chung K-W, Zuchner S, Pareyson D, Harms M, Reilly Mary M, Houlden H (2014) Truncating and missense mutations in IGHMBP2 cause Charcot-Marie-Tooth disease type 2. Am J Hum Genet 95:590–601
6. Ylikallio E, Woldegebriel R, Tumiati M, Isohanni P, Ryan MM, Stark Z, Walsh M, Sawyer SL, Bell KM, Oshlack A, Lockhart PJ, Shcherbii M, Estrada-Cuzcano A, Atkinson D, Hartley T, Tetreault M, Cuppen I, Ludo van der Pol W, Candayan A, Battaloglu E, Parman Y, van Gassen KLI, van den Boogaard M-JH, Boycott KM, Kauppi L, Jordanova A, Lönnqvist T, Tyynismaa H (2017) *MCM3AP* in recessive Charcot-Marie-Tooth neuropathy and mild intellectual disability. Brain 140(8):2093–2103
7. Lindner TH, Hoffmann K (2005) easyLINKAGE: a PERL script for easy and automated two-/multi-point linkage analyses. Bioinformatics 21:405–407
8. Abecasis GR, Cherny SS, Cookson WO, Cardon LR (2002) Merlin–rapid analysis of dense genetic maps using sparse gene flow trees. Nat Genet 30:97–101
9. Cottingham RW, Idury RM, Schäffer AA (1993) Faster sequential genetic linkage computations. Am J Hum Genet 53:252–263
10. Matise TC, Chen F, Chen W, De La Vega FM, Hansen M, He C, Hyland FC, Kennedy GC, Kong X, Murray SS, Ziegle JS, Stewart WC, Buyske S (2007) A second-generation combined linkage physical map of the human genome. Genome Res 17:1783–1786
11. Drew AP, Zhu D, Kidambi A, Ly C, Tey S, Brewer MH, Ahmad-Annuar A, Nicholson GA, Kennerson ML (2015) Improved inherited peripheral neuropathy genetic diagnosis by whole-exome sequencing. Mol Genet Genomic Med 3:143–154
12. Bahlo M, Bromhead CJ (2009) Generating linkage mapping files from Affymetrix SNP chip data. Bioinformatics 25:1961–1962
13. Purcell S, Neale B, Todd-Brown K, Thomas L, Ferreira MAR, Bender D, Maller J, Sklar P, de Bakker PIW, Daly MJ, Sham PC (2007) PLINK: a tool set for whole-genome association and population-based linkage analyses. Am J Hum Genet 81:559–575
14. Blankenberg D, Von Kuster G, Coraor N, Ananda G, Lazarus R, Mangan M, Nekrutenko A, Taylor J (2010) Galaxy, a web-based genome analysis tool for experimentalists. Curr Protoc Mol Biol 0(19):Unit-19.1021
15. Goecks J, Nekrutenko A, Taylor J, Team TG (2010) Galaxy: a comprehensive approach for supporting accessible, reproducible, and transparent computational research in the life sciences. Genome Biol 11:R86
16. Tey S, Ahmad-Annuar A, Drew AP, Shahrizaila N, Nicholson GA, Kennerson ML (2016) Mutation analysis of genes within the dynactin complex in a cohort of hereditary peripheral neuropathies. Clin Genet 90:127–133
17. Schmittgen TD, Livak KJ (2008) Analyzing real-time PCR data by the comparative CT method. Nat Protocols 3:1101–1108
18. Shahrizaila N, Samulong S, Tey S, Suan LC, Meng LK, Goh KJ, Ahmad-Annuar A (2014) X-linked Charcot-Marie-Tooth disease predominates in a cohort of multiethnic Malaysian patients. Muscle Nerve 49:198–201
19. Kircher M, Witten DM, Jain P, O'Roak BJ, Cooper GM, Shendure J (2014) A general framework for estimating the relative pathogenicity of human genetic variants. Nat Genet 46(3):310–315
20. Narasimhan VM, Hunt KA, Mason D, Baker CL, Karczewski KJ, Barnes MR, Barnett AH, Bates C, Bellary S, Bockett NA, Giorda K, Griffiths CJ, Hemingway H, Jia Z, Kelly MA, Khawaja HA, Lek M, McCarthy S, McEachan R, O'Donnell-Luria A, Paigen K, Parisinos CA, Sheridan E, Southgate L, Tee L, Thomas M, Xue Y, Schnall-Levin M, Petkov PM, Tyler-Smith C, Maher ER, Trembath RC, MacArthur DG, Wright J, Durbin R, van Heel DA (2016) Health and population effects of rare gene knockouts in adult humans with related parents. Science 352:474–477
21. Sano K, Miura S, Fujiwara T, Fujioka R, Yorita A, Noda K, Kida H, Azuma K, Kaieda S, Yamamoto K, Taniwaki T, Fukumaki Y, Hiroki S (2015) A novel missense mutation of RYR1 in familial idiopathis hyper CK-emia. J Neurol Sci 356(1–2):142–147
22. Nagata K, Takahashi M, Kiryu-Seo S, Hiroshi K, Saido TC (2017) Distinct functional consequences of ECEL1/DINE missense mutations in the pathogenesis of congenital contracture disorders. Acta Neuropathol Commun 5:83
23. Komuro A, Masuda Y, Kobayashi K, Babbitt R, Gunel M, Flavell RA, Marchesi VT (2004) The AHNAKs are a class of giant propeller-like proteins that associate with calcium channel proteins of cardiomyocytes and other cells. Proc Natl Acad Sci U S A 101:4053–4058
24. Luzón-Toro B, Gui H, Ruiz-Ferrer M, Sze-Man Tang C, Fernández RM, Sham P-C, Torroglosa A, Kwong-Hang Tam P, Espino-Paisán L, Cherny SS, Bleda M, Enguix-Riego MV, Dopazo J, Antiñolo G, García-Barceló M-M, Borrego S (2015) Exome sequencing reveals a high genetic heterogeneity on familial Hirschsprung disease. Sci Rep 5:16473
25. Monies D, Abouelhoda M, AlSayed M, Alhassnan Z, Alotaibi M, Kayyali H, Al-Owain M, Shah A, Rahbeeni Z, Al-Muhaizea MA, Alzaidan HI, Cupler E, Bohlega S, Faqeih E, Faden M, Alyounes B, Jaroudi D, Goljan E, Elbardisy H, Akilan A, Albar R, Aldhalaan H, Gulab S, Chedrawi A, Al Saud BK, Kurdi W, Makhseed N, Alqasim T, El Khashab HY, Al-Mousa H, Alhashem A, Kanaan I, Algoufi T, Alsaleem K, Basha TA, Al-Murshedi F, Khan S, Al-Kindy A, Alnemer M, Al-Hajjar S, Alyamani S, Aldhekri H, Al-Mehaidib A, Arnaout R, Dabbagh O, Shagrani M, Broering D, Tulbah M, Alqassmi A, Almugbel M, AlQuaiz M, Alsaman A, Al-Thihli K, Sulaiman RA, Al-Dekhail W, Alsaegh A, Bashiri FA, Qari A, Alhomadi S, Alkuraya H, Alsebayel M, Hamad MH, Szonyi L, Abaalkhail F, Al-Mayouf SM, Almojalli H, Alqadi KS, Elsiesy H, Shuaib TM, Seidahmed MZ, Abosoudah I, Akleh H, AlGhonaium A, Alkharfy TM, Al Mutairi F, Eyaid W, Alshanbary A, Sheikh FR, Alsohaibani FI, Alsonbul A, Al Tala S, Balkhy S, Bassiouni R, Alenizi AS, Hussein MH, Hassan S, Khalil M, Tabarki B, Alshahwan S, Oshi A, Sabr Y, Alsaadoun S, Salih MA, Mohamed S, Sultana H, Tamim A, El-Haj M, Alshahrani S, Bubshait DK, Alfadhel M, Faquih T, El-Kalioby M, Subhani S, Shah Z, Moghrabi N, Meyer BF, Alkuraya FS (2017) The landscape of genetic diseases in Saudi Arabia based on the first 1000 diagnostic panels and exomes. Hum Genet 136:921–939
26. Marg A, Haase H, Neumann T, Kouno M, Morano I (2010) AHNAK1 and AHNAK2 are costameric proteins: AHNAK1 affects transverse skeletal muscle fiber stiffness. Biochem Biophys Res Commun 401:143–148
27. Hohaus A, Person V, Behlke J, Schaper J, Morano I, Haase H (2002) The carboxyl-terminal region of ahnak provides a link between cardiac L-type Ca2+ channels and the actin-based cytoskeleton. FASEB J 16:1205–1216
28. Huang Y, Laval SH, van Remoortere A, Baudier J, Benaud C, Anderson LVB, Straub V, Deelder A, Frants RR, den Dunnen JT, Bushby K, van der Maarel SM (2007) AHNAK, a novel component of the dysferlin protein complex, redistributes to the cytoplasm with dysferlin during skeletal muscle regeneration. FASEB J 21:732–742

29. Davies TA, Loos B, Engelbrecht AM (2014 Dec) AHNAK: the giant jack of all trades. Cell Signal 26(12):2683–2693
30. Han H, Kursula P (2014) Periaxin and AHNAK nucleoprotein 2 form intertwined homodimers through domain swapping. J Biol Chem 289:14121–14131
31. Gillespie CS, Sherman DL, Blair GE, Brophy PJ (1994) Periaxin, a novel protein of myelinating Schwann cells with a possible role in axonal ensheathment. Neuron 12:497–508
32. Guilbot A, Williams A, Ravise N, Verny C, Brice A, Sherman DL, Brophy PJ, LeGuern E, Delague V, Bareil C, Megarbane A, Claustres M (2001) A mutation in periaxin is responsible for CMT4F, an autosomal recessive form of Charcot-Marie-Tooth disease. Hum Mol Genet 10:415–421
33. Boerkoel CF, Takashima H, Stankiewicz P, Garcia CA, Leber SM, Rhee-Morris L, Lupski JR (2001) Periaxin mutations cause recessive Dejerine-Sottas neuropathy. Am J Hum Genet 68:325–333
34. Kirov A, Kacer D, Conley BA, Vary CP, Prudovsky I (2015) AHNAK2 participates in the stress-induced nonclassical FGF1 secretion pathway. J Cell Biochem 116:1522–1531
35. Hossain WA, Morest DK (2000) Fibroblast growth factors (FGF-1, FGF-2) promote migration and neurite growth of mouse cochlear ganglion cells in vitro: immunohistochemistry and antibody perturbation. J Neurosci Res 62:40–55

Affiliations

Shelisa Tey[1] · Nortina Shahrizaila[2] · Alexander P. Drew[3,4] · Sarimah Samulong[1] · Khean-Jin Goh[2] · Esra Battaloglu[5] · Derek Atkinson[6] · Yesim Parman[7] · Albena Jordanova[6] · Ki Wha Chung[8] · Byung-Ok Choi[9] · Yi-Chung Li[10] · Michaela Auer-Grumbach[11] · Garth A. Nicholson[3,4,12] · Marina L. Kennerson[3,4,12] · Azlina Ahmad-Annuar[1]

[1] Department of Biomedical Science, Faculty of Medicine, University of Malaya, 50603 Kuala Lumpur, Malaysia

[2] Department of Medicine, Faculty of Medicine, University of Malaya, 50603 Kuala Lumpur, Malaysia

[3] Northcott Neuroscience Laboratory, ANZAC Research Institute, University of Sydney, Concord, NSW, Australia

[4] Sydney Medical School, University of Sydney, Sydney, NSW, Australia

[5] Department of Molecular Biology and Genetics, Bogazici University, Istanbul, Turkey

[6] Molecular Neurogenomics Group, VIB-U Antwerp Center for Molecular Neurology, University of Antwerp, 2610 Antwerpen, Belgium

[7] Department of Neurology, Istanbul School of Medicine, Istanbul University, Istanbul, Turkey

[8] Department of Biological Sciences, Kongju National University, Gongju, South Korea

[9] Department of Neurology, Samsung Medical Center, Sungkyunkwan University School of Medicine, Seoul, South Korea

[10] Department of Neurology, Taipei Veterans General Hospital, National Yang-Ming University School of Medicine, Taipei 11221, Taiwan

[11] Department of Orthopedics and Trauma Surgery, Medical University of Vienna, 1090 Vienna, Austria

[12] Molecular Medicine Laboratory, Concord Hospital, Concord, NSW, Australia